RSC Advances

PAPER

View Article Online
View Journal | View Issue

Cite this: *RSC Adv.*, 2014, **4**, 43590

Antifouling behaviours of PVDF/nano-TiO_2 composite membranes revealed by surface energetics and quartz crystal microbalance monitoring†

Qiaoying Wang, Zhiwei Wang,* Jie Zhang, Jie Wang and Zhichao Wu

Received 18th July 2014
Accepted 5th September 2014

DOI: 10.1039/c4ra07274j

www.rsc.org/advances

Poly(vinylideneflouride) (PVDF)/nano-titanium dioxide (TiO_2) composite membranes were prepared *via* a phase inversion method by dosing different amounts of TiO_2 nanoparticles in PVDF casting solution to improve the antifouling ability. The extended Derjaguin–Landau–Verwey–Overbeek (XDLVO) theory and the quartz crystal microbalance with dissipation (QCM-D) monitoring were adopted to clarify the antifouling behaviours of the composite membranes. The results showed that the addition of nano-TiO_2 could improve the membrane surface porosity, volume porosity, hydrophilicity and permeability. The electron donor monopolarity of the composite membranes was evidently enhanced, and the repulsive interaction energy barrier between foulants and membrane surfaces was increased by adding TiO_2 nanoparticles, thus improving the antifouling ability. The optimal dosage of TiO_2 nanoparticles was 0.05 wt% for the composite membranes. It was also found that when the TiO_2 concentration was higher than 0.05 wt%, the aggregated TiO_2 nanoparticles dispersed inside the membrane increased the roughness of the pore wall and lowered the energy barrier between foulants and the membrane inner surface, which allowed more foulants to adsorb into the membrane pores.

1. Introduction

Although membrane separation technology has been commonly applied worldwide for water and wastewater treatment,[1,2] membrane fouling is still a critical factor hindering the practical application of membrane technology. Therefore, to improve membrane antifouling properties has attracted much attention in the past decades.[3] Many strategies such as surface graft polymerization, chemical grafting, surface coating and additive dosing have been adopted to modify membrane characteristics.[4] Among these methods, introduction of inorganic nanoparticles into polymeric membranes to form organic/inorganic composite membranes have shown significant effectiveness in improving membrane hydrophilicity, changing pore structure, and enhancing membrane antifouling ability.[5]

Various inorganic nanomaterials including TiO_2,[6,7] SiO_2,[8] ZrO_2,[9] Al_2O_3,[10] zeolite nanoparticles,[11] graphene oxides,[12] and carbon nanotubes[13] have been used to fabricate composite membranes. Among these inorganic nanoparticles, nano-sized TiO_2 has received much attention due to its high hydrophilicity, great chemical stability, and antibacterial property.[14] Oh *et al.*[15] modified poly(vinylideneflouride) (PVDF) ultrafiltration (UF) membrane by dispersing nano-sized TiO_2 in a PVDF solution, and their results indicated that PVDF membrane fouling was reduced due to the enhancement of hydrophilicity after TiO_2 addition. Cao *et al.*[16] found that the membrane surface became smoother through the addition of nanoparticles. Li *et al.*[6] reported that thermal stability of the composite membrane had been improved by the addition of TiO_2 nanopaticles. They also found that the composite membrane had a top surface with high porosity at low loading amount of TiO_2; however, at higher loading, the skin layer became much looser because of a significant aggregation of TiO_2 nanopaticles. The work of Yang *et al.*[17] also showed that the water permeability, hydrophilicity, mechanical strength and antifouling ability of the composite membrane was significantly enhanced by the addition of TiO_2 nanoparticles.

Although the addition of TiO_2 nanoparticles into the casting solution has been proven to improve the antifouling ability, a systematical investigation of mechanisms improving membrane antifouling behaviours of the composite membranes is still lacking. It is mainly attributed to that the presence of TiO_2 nanoparticles can result in the changes of hydrophilicity, zeta potential, roughness and porosity simultaneously. All of those factors have their positive or negative influences on membrane fouling behaviours. It is of

State Key Laboratory of Pollution Control and Resource Reuse, School of Environmental Science and Engineering, Tongji University, Shanghai 200092, P.R. China. E-mail: zwwang@tongji.edu.cn; Fax: +86 (21)65980400; Tel: +86 (21) 65980400

† Electronic supplementary information (ESI) available. See DOI: 10.1039/c4ra07274j

significance to establish a comprehensive understanding of the antifouling behaviours for the composite membranes by taking all of factors into consideration.

In this study, TiO_2 nanoparticles with a series of dosages were introduced into PVDF materials to prepare PVDF/TiO_2 composite membranes. The physicochemical properties of the composite membranes were characterized by scanning electron microscope (SEM), energy-diffusive X-ray analyzer (EDX), atomic force microscopy (AFM) and attenuated total reflectance Fourier transform infrared (ATR-FTIR). The membrane surface energetics (free energy and interaction energy between membranes and foulants) was assessed by extended Derjaguin–Landau–Verwey–Overbeek (XDLVO) theory in order to unifying the overall influences of membrane physicochemical factors. The antifouling behaviours were further determined by quartz crystal microbalance with dissipation (QCM-D) technology. The obtained results are expected to provide a sound understanding on the antifouling behaviours of PVDF/TiO_2 composite membranes.

2. Materials and methods

2.1. Materials

Commercial grade PVDF (FR904) was purchased from Shanghai 3F New Materials Ltd. (Shanghai, China). Dimethylacetamide (DMAC) and polyethylene glycol (PEG, 400 Da) used as the solvent and pore-forming additive, respectively, were supplied by Sinopharm (Shanghai, China). TiO_2 reagent with diameters of 10–50 nm and purity of 99.8% was obtained from Hangzhou Wanjing New Materials Co., Ltd. (Hangzhou, China). Soluble microbial products (SMP) have been reported to be the major membrane foulants in membrane bioreactors.[18,19] SMP mainly contains polysaccharides, proteins, humic acids, nucleic acids, and other polymeric compounds, among which polysaccharides are known as the dominant foulants due to their macromolecular characteristics.[20,21] In this study, sodium alginate (SA) supplied by Sigma Aldrich was adopted as model SMP-foulants at a concentration of 500 mg L^{-1}. NaCl was used to adjust the ionic strength of the SA solution. pH was controlled with HCl and NaOH. Deionized water was used throughout this study.

2.2. Membrane preparation

The pristine PVDF membrane and PVDF/TiO_2 composite membranes were prepared by the phase inversion method. Predetermined dosages of TiO_2 nanoparticles were dispersed in 85 g DMAC in a beaker and bath-sonicated for 1 h. PVDF was dried at 80 °C for 24 h to eliminate the absorbed water molecules before the preparation, and then 8 g PVDF and 7 g PEG were completely dissolved in the DMAC solvent. PEG has been widely used as a good pore former during the fabrication of ultrafiltration/microfiltration membrane due to its high hydrophilicity.[22,23] The casting solutions were dissolved at 80 °C for 48 h to form homogeneous solutions. The homogeneous casting solutions were subsequently casted on a glass plate and the scraper clearance was controlled at 250 μm, and then were shortly (generally 30 s) exposed to ambient air (20 ± 1 °C, 30 ± 5% relative humidity) to allow partial evaporation of the solvents. After that, these solution films together with the glass plate were moved toward the non-solvent bath for immersion precipitation at room temperature. In this study, water was used as the non-solvent bath media and the water temperature was maintained at 25 ± 1 °C. Phase inversion started immediately, and then the solid membrane was detached from the glass plate. The obtained membranes were then repeatedly washed with water and immersed in distilled water for the subsequent analysis. The PVDF/TiO_2 membranes made from the casting solutions with 0.02, 0.05, 0.10 and 0.50 wt% TiO_2 were named as T-0.02, T-0.05, T-0.1 and T-0.5, respectively. The pristine PVDF membrane was termed T-0 as a control.

2.3. Membrane properties

The SEM and EDX analyses were carried out with an SEM and its adjunct EDX analyzer (Model XL-30, Philips, Netherlands) to characterize the membrane morphologies and elemental compositions of membrane samples, respectively. The membrane topography was also determined by AFM technology (Multimode IV, Bruker Nano Surface, USA) and the Nanoscope® control software was used for image acquisition. The average roughness (R_a), root mean-square roughness (R_q) and maximum roughness (R_m) were determined to quantitatively compare the variations. R_a is the average deviation of the measured z-values from the basic plane, which is thought of as half the average peak-to-valley depth. R_q indicates the standard deviation of an entire distribution of z-values for a large sample size, and R_m represents the difference between the largest positive and negative z-values. To study the surface chemical composition changes of the PVDF membranes, ATR-FTIR spectra were collected using a Nicolet 5700 spectrometer (Thermo Electron Corporation, USA) set at a 4 cm^{-1} resolution. The spectra were measured at wavenumbers in the range of 1500–700 cm^{-1}. The measurements of the membrane volume porosity and pure water flux were conducted according to our previous report.[24] The membrane volume porosity is defined as the pores' volume divided by the total volume of the membrane and was determined by gravimetric method. 20 mm × 20 mm membrane specimens were used and three measurements for each sample were carried out. Pure water flux was determined by dead-end filtration method. All membrane samples were subject to the compaction under a *trans*-membrane pressure (TMP) of 1.0 bar until the flux was stable. Then, the filtrate of 17.3 cm^2 membrane sample was collected for 2 min under the TMP of 0.03 bar to calculate the pure water flux. The pure water flux was reported by averaging three measurements for each membrane at room temperature (25 ± 1 °C).

Contact angle was measured using an optical contact angle measurement system (OCA 15 Plus, Data physics GmbH, Germany). Each reported value was expressed by averaging five measurements of different positions for each sample.

2.4. XDLVO theory

In this study, XDLVO theory was employed to assess the interaction energetics between foulants and membrane surfaces. According to van Oss,[25] the energy balances for aqueous system are determined by the sum of Lifshitz–van der Waals (LW),

electrostatic (EL) and acid–base (AB) interaction energy, which can be expressed by eqn (1).

$$U_{\mathrm{mlc}}^{\mathrm{XDLVO}} = U_{\mathrm{mlc}}^{\mathrm{LW}} + U_{\mathrm{mlc}}^{\mathrm{EL}} + U_{\mathrm{mlc}}^{\mathrm{AB}} \quad (1)$$

In eqn (1), $U_{\mathrm{mlc}}^{\mathrm{LW}}$, $U_{\mathrm{mlc}}^{\mathrm{EL}}$ and $U_{\mathrm{mlc}}^{\mathrm{AB}}$ are the individual components of the total interfacial energy associated with LW, EL and AB forces, respectively. The subscripts m, l and c refer to membrane, bulk liquid (*i.e.*, water in this study) and foulants (*i.e.*, alginate in this study), respectively. These components' interfacial energy could be calculated as follows.

$$U_{\mathrm{mlc}}^{\mathrm{LW}} = 2\pi\Delta G_{h_0}^{\mathrm{LW}} \frac{{h_0}^2 a}{h} \quad (2)$$

$$U_{\mathrm{mlc}}^{\mathrm{AB}} = 2\pi a\lambda\Delta G_{h_0}^{\mathrm{AB}} \exp\left[\frac{h_0 - h}{h}\right] \quad (3)$$

$$U_{\mathrm{mlc}}^{\mathrm{EL}} = \pi\varepsilon a\left[2\xi_{\mathrm{c}}\xi_{\mathrm{m}} \ln\left(\frac{1+\mathrm{e}^{-kh}}{1-\mathrm{e}^{kh}} + \left(\xi_{\mathrm{c}}{}^2 + \xi_{\mathrm{m}}{}^2\right)\ln\left(1-\mathrm{e}^{-2kh}\right)\right)\right] \quad (4)$$

In the above equations, a is the radius of foulant, h the separation distance between membrane and foulants, λ the decay length of AB interactions (0.6 nm in aqueous systems).[26] ε is the dielectric permittivity of the suspending fluid, κ the inverse Debye screening length, and ξ_{m} and ξ_{c} are the surface potentials of the membrane and foulant, respectively. $\Delta G_{h_0}^{\mathrm{LW}}$ and $\Delta G_{h_0}^{\mathrm{AB}}$ are the Liftshitz–van der Waals and acid–base interaction free energy components at the separation distance of h_0, respectively, whereas the subscript h_0 refers to the minimum separation distance of 0.158 nm.[25] $\Delta G_{h_0}^{\mathrm{LW}}$ and $\Delta G_{h_0}^{\mathrm{AB}}$ can be worked out by eqn (5) and (6), respectively.[26]

$$\Delta G_{h_0}^{\mathrm{LW}} = 2\left(\sqrt{\gamma_{\mathrm{l}}^{\mathrm{LW}}} - \sqrt{\gamma_{\mathrm{m}}^{\mathrm{LW}}}\right)\left(\sqrt{\gamma_{\mathrm{c}}^{\mathrm{LW}}} - \sqrt{\gamma_{\mathrm{l}}^{\mathrm{LW}}}\right) \quad (5)$$

$$\begin{aligned}\Delta G_{h_0}^{\mathrm{AB}} =& 2\sqrt{\gamma_{\mathrm{l}}^{+}}\left(\sqrt{\gamma_{\mathrm{m}}^{-}} + \sqrt{\gamma_{\mathrm{c}}^{-}} - \sqrt{\gamma_{\mathrm{l}}^{-}}\right) \\ &+ 2\sqrt{\gamma_{\mathrm{l}}^{-}}\left(\sqrt{\gamma_{\mathrm{m}}^{+}} + \sqrt{\gamma_{\mathrm{c}}^{+}} - \sqrt{\gamma_{\mathrm{l}}^{+}}\right) - 2\left(\sqrt{\gamma_{\mathrm{m}}^{+}\gamma_{\mathrm{c}}^{-}} + \sqrt{\gamma_{\mathrm{m}}^{-}\gamma_{c}^{+}}\right)\end{aligned} \quad (6)$$

where γ^{LW} is the LW component, γ^{+} the electron acceptor parameter and γ^{-} the electron donor parameter. The surface tension parameters ($\gamma_{\mathrm{s}}^{\mathrm{LW}}$, γ_{s}^{+}, γ_{s}^{-}) of the membrane and alginate could be obtained using the extended Young's equation.[28] The extended Young's equation describes the relationship between the contact angle of a liquid on a solid surface and the surface tension parameters of both the solid and the liquid, which can be written as follows.[27–29]

$$(1+\cos\theta)\gamma_{\mathrm{l}}^{\mathrm{TOT}} = 2\left(\sqrt{\gamma_{\mathrm{s}}^{\mathrm{LW}}\gamma_{\mathrm{l}}^{\mathrm{LW}}} + \sqrt{\gamma_{\mathrm{s}}^{+}\gamma_{\mathrm{l}}^{-}} + \sqrt{\gamma_{\mathrm{s}}^{-}\gamma_{\mathrm{l}}^{+}}\right) \quad (7)$$

where θ is the contact angle, and the subscripts s and l correspond to the solid surface and the liquid, respectively. The left side of the equation means the free energy of cohesion per unit area of the liquid (l), while the right side represents the free energy of adhesion per unit area between the liquid (l) and the solid (s).[26,30] γ^{TOT} is the total surface tension, which is equal to the sum of LW (apolar) and AB (polar) components as given by eqn (8).[27]

$$\gamma^{\mathrm{TOT}} = \gamma^{\mathrm{LW}} + \gamma^{\mathrm{AB}} \quad (8)$$

The apolar LW component shows a single electrodynamic property of a given material, whereas the polar AB component comprises two non-additive electron acceptor and electron donor parameters.[26,31] The polar AB component of a material's surface free energy is expressed by eqn (9).[32]

$$\gamma^{\mathrm{AB}} = 2\sqrt{\gamma^{+}\gamma^{-}} \quad (9)$$

The specific measurement and calculation procedure of surface energetics parameters for XDLVO theory can be found in ESI (the text and Tables S1–S4†).

2.5. QCM-D measurements

QCM-D was used to dynamically examine the adsorption behaviors of the model SMP-foulants on the PVDF and PVDF/TiO_2 composite membranes by monitoring the change of the oscillation frequency (Δf) when SA was flowing above the polymer-coated QCM-D crystal with a Q-Sense E4 unit (Q-Sense AB, Göteborg, Sweden).

Firstly, 10-fold dilutions of the homogeneous casting solutions of T-0–T-0.5 membranes were performed with DMAC. The gold-coated crystal sensors with a fundamental resonant frequency of 4.95 MHz and a diameter of 14 mm were pre-cleaned using 10 wt% sodium dodecyl sulfate (Sinopharm, Shanghai, China), and then rinsed thoroughly with deionized water and dried with pure nitrogen. Then, the sensors were spin-coated with the diluted polymer solutions at 6000 rpm for 60 s (KW-4A, Chemat Technology, USA), followed by drying on a hot plate (DB-3, Changzhou Guohua Electric Appliance Co., Ltd, China) at 353 K for 30 min. 500 mg L^{-1} SA solution with 10 mM NaCl under pH = 6.5 was used as model foulants, and 10 mM NaCl under pH = 6.5 was used as background solution. The aqueous media was injected into the QCM-D flow-cell at 150 μL min^{-1} flow rate with a peristaltic pump (IsmaTec pump, IDEX). The stages for applying aqueous media to the QCM-D flow-cell include the following 5 steps: (A) deionized water; (B) background solution; (C) SA solution; (D) background solution; (E) deionized water. Each step was maintained for 15 min at constant temperature (25 °C) after acquiring a stable baseline with deionized water for several hours. The variation of frequency at the seventh overtone was observed to analyze the adsorption rate.

3. Results and discussion

3.1. Physicochemical properties of the composite membranes

3.1.1. Membrane morphologies. The surface and cross-sectional morphologies of the membranes are shown in Fig. 1. All the membranes exhibited the porous top layer and interconnected macrovoid structure in the cross-section images. The surface porosity of the PVDF/TiO_2 composite membrane was obvious greater than that of the original PVDF

membrane (Fig. 1), and TiO_2 particles could not be observed on the toplayer. However, the aggregated TiO_2 particles (about 0.2–1.0 μm) were found dispersed in the cross-sections of the T-0.1 and T-0.5 membranes as shown in Fig. 1(h) and (j), indicating that the aggregation of TiO_2 nanoparticles occurred at higher dosages. According to previous studies, the critical concentration of TiO_2 causing aggregation was different with different compositions of the casting solutions. Yang *et al.*[17] observed nano-TiO_2 aggregated at concentration of 2 wt% in preparing the polysulfone (PSF)/TiO_2 organic–inorganic composite ultrafiltration membranes. Vatanpour *et al.*[33] reported that aggregation of nano-TiO_2 with average crystalline size of 25 nm occurred when the concentration was larger than 4 wt% and the critical concentration was different for the nano-TiO_2 with different sizes. It could be inferred that the critical concentration of nanoparticles to aggregate in membrane casting solutions could be influenced by the interaction of nanoparticle and polymer, nanoparticle and solvent, and also the inherent properties of nanoparticles.

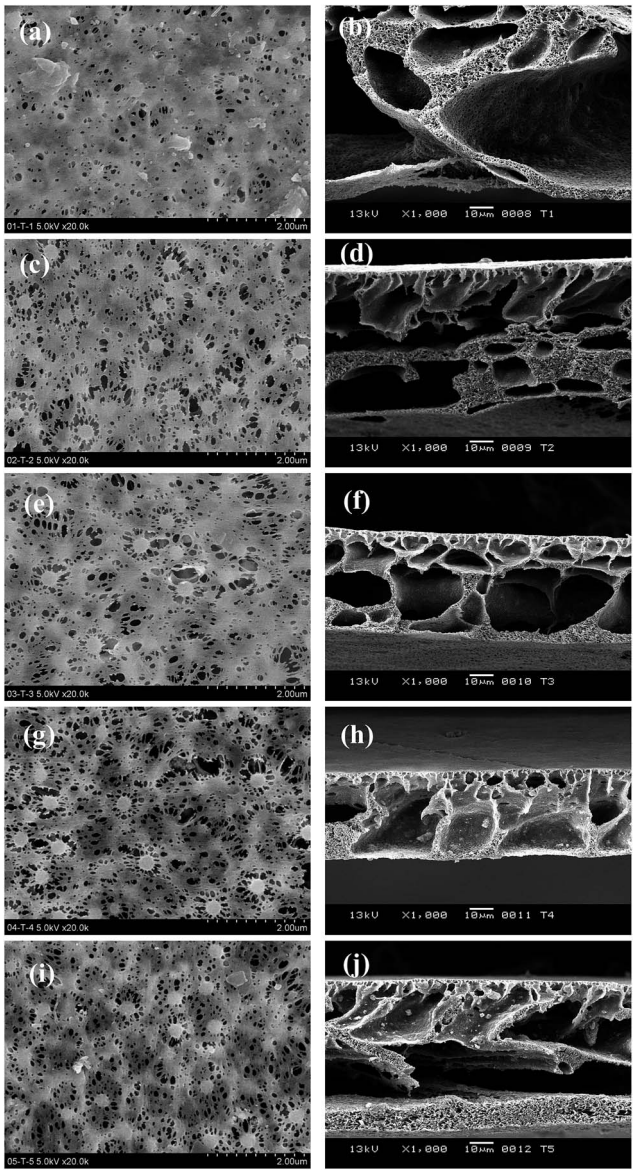

Fig. 1 SEM micrographs of all the membranes. (a), (c), (e), (g), and (i) are the surface images of T-0, T-0.02, T-0.05, T-0.1, and T-0.5; (b), (d), (f), (h), and (j) are the cross-section images of T-0–T-0.5, respectively.

According to the membrane formation mechanisms, once the casting solution and nonsolvent comes into contact, a skin layer forms immediately because the mutual diffusion between solvent in the casting solution and non-solvent in the coagulation bath. When the amount of nonsolvent diffused into the casting solution is sufficient to destabilize thermodynamically stability somewhere, the casting solution reduces its free energy from dividing into two liquid phases of different composition, *i.e.*, a nucleus of the polymer-poor phase that forms the nascent pore and a polymer-rich phase that surrounds the pore. In other words, the polymer precipitation takes place at this moment. When more non-solvent enters the different sites of the skin layer, more pores appear. Since nano-TiO_2 has the higher affinity to water compared to that of PVDF, penetration velocity of water (non-solvent) into the nascent membrane can be enhanced by the addition of TiO_2 during the phase inversion, which is supposed to accelerate the formation of surface pores. In addition, due to the fact that the interaction between polymers and solvent molecules could be hindered by the obstruction of nanoparticles, it can therefore increase the solvent (DMAC) diffusion velocity from the membrane to water,[34] which also contributed to the formation of micropores on the membrane surface. Therefore, the average pore size and porosity of PVDF/nano-TiO_2 composite membranes was higher than that of the original PVDF membrane.

In order to further examine the effects of TiO_2 nanoparticles on the membrane surface roughness, AFM analyses were performed for all the membranes. The three-dimensional AFM images are shown in Fig. S1 of the ESI† and the roughness is illustrated in Fig. 2. It could be observed that all the membranes have similar magnitude of asperity in their surfaces. The R_a and R_q values of all the membranes were about 72.2–78.6 nm and 58.0–59.7 nm, respectively, showing that the membrane surface roughness was not obviously changed with the addition of TiO_2 nanoparticles in this study. However, *R*m was generally enlarged with the increase of TiO_2 dosages. This result indicates that the existence of insoluble aggregated TiO_2 particles in the matrix might turn into a bump in the sub-layer during membrane preparation and increase the peak value of the asperity.

3.1.2. TiO_2 distribution and functional group detection. To determine the dispersion of TiO_2 in the composite membrane, EDX analysis was carried out and the weight (Wt) percentage of C, O, F and Ti on the top layer of all the membranes is shown in Fig. 3. Titanium was detected dispersed on the top layer of composite membranes, and the determined concentration of titanium was quite consistent with the theoretic value which was calculated by the mass ratios of titanium and PVDF. This result might reveal that the TiO_2 nanoparticles were uniformly distributed into casting solutions during composite membrane preparation.

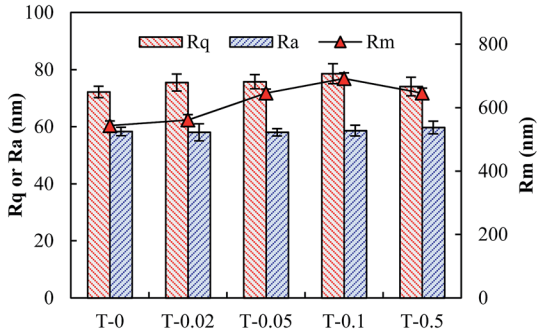

Fig. 2 The average roughness (R_a), root mean-square roughness (R_q) and maximum roughness (R_m) of the membranes obtained from AFM images.

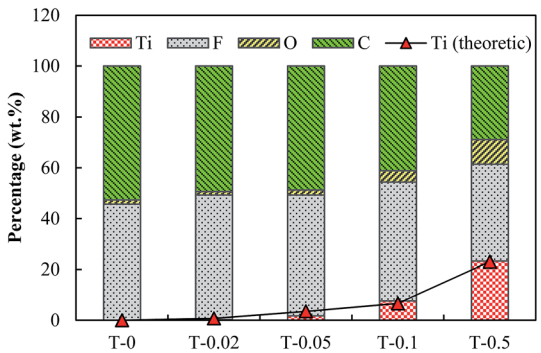

Fig. 3 EDX analysis of all the membranes.

Fig. 4 shows the ATR-FTIR spectra of PVDF membrane and PVDF/TiO_2 composite membranes. The absorption peak at 1180 cm^{-1} is assigned to the stretching vibration of CF_2 groups, and the deformed vibration of CH_2 groups appears at the frequency of 1402 cm^{-1}.[35] FTIR spectra of two major phases (α and β phases) of PVDF have been intensively investigated. In this study, the vibrational bands at 765 cm^{-1} (CF_2 bending and skeletal bending), 795 cm^{-1} (CH_2 rocking), 874 cm^{-1} and 974 cm^{-1} are associated with α-phase,[36–38] and the vibrational bands at 840 cm^{-1} (CH_2 rocking) correspond to β-phase. It was also visible that the absorption peak of α-phase was gradually reduced with the addition of TiO_2, and disappeared when the amount of TiO_2 was 0.5 wt%. On the contrary, the adsorption peak of β-phase was enhanced by the addition of TiO_2. These results showed that the addition of TiO_2 nanoparticles increased the content of β-phase crystallize of PVDF, and in the meantime reduced that of α-phase. Andrew and Clarke[39] detected the melting temperature (T_m) of PVDF electrospun samples with different crystalline phase by measuring the melting enthalpy using differential scanning calorimetry (DSC). They reported that the variation of T_m was mainly due to the change in the relative amounts of the β and α phases, and an increased contribution from the lower melting α-phase could induce the decrease in T_m, *i.e.*, the decrease of thermal stability. According to their results, it can be inferred that the thermal stability of composite membrane has been enhanced by the addition of TiO_2 nanoparticles in this study.

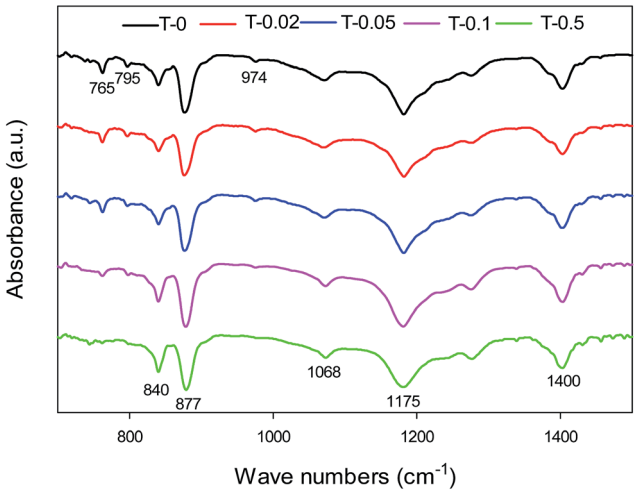

Fig. 4 FTIR spectra of PVDF/TiO_2 composite membranes and original PVDF membrane.

3.1.3. Membrane porosity, contact angle and pure water flux. The volume porosity, contact angle and pure water flux of the original PVDF membrane and the PVDF/TiO_2 composite membranes were compared to illustrate the influences of nano-sized TiO_2 on the physicochemical properties of the membranes. It could be observed from Fig. 5(a) that the membrane porosity was improved by the addition of TiO_2, and the improvement was most significant when the dosage was 0.05 wt%. Based on membrane formation kinetics, at a slower exchange velocity between solvent and non-solvent through the coagulation and top-layer when the polymer film is immersed in a coagulation bath, the polymer-lean phase growth and coalescence will be more rapidly developed, thus forming larger finger-like pores.[40] Compared to PVDF, TiO_2 has higher affinity with water (*i.e.*, non-solvent in this study), and the fast diffusion rate between TiO_2 and water results in a delay of the exchange between the non-solvent bath and the polymer casting film before gelation and vitrification of the polymer, allowing more cross-sectional pores formed and coalesced into microvoids. However, with the further increase of TiO_2 dosage in the polymeric matrix, the volume porosity of the composite membrane decreased. That is due to that the further addition of TiO_2 results in the increase of the total solid content in the casting solution, which has been known to reduce the membrane porosity.[6] Furthermore, aggregated TiO_2 nanoparticles could block the membrane pores, subsequently reducing the membrane porosity. The contact angle between water and the prepared membrane surface was measured to evaluate the membrane hydrophilicity. Fig. 5(a) manifests that the contact angle of original PVDF membrane is the highest (86°), and the contact angle of PVDF/TiO_2 composite membrane is generally reduced to 71–75° by the addition of TiO_2. This demonstrates that the addition of TiO_2 enhances the hydrophilicity of membrane which is consistent with the previous reports.[33,41] As shown in Fig. 5(b), the pure water flux of the composite membranes gradually improved when the amount of the TiO_2 nanoparticles was increased in the casting solution, suggesting

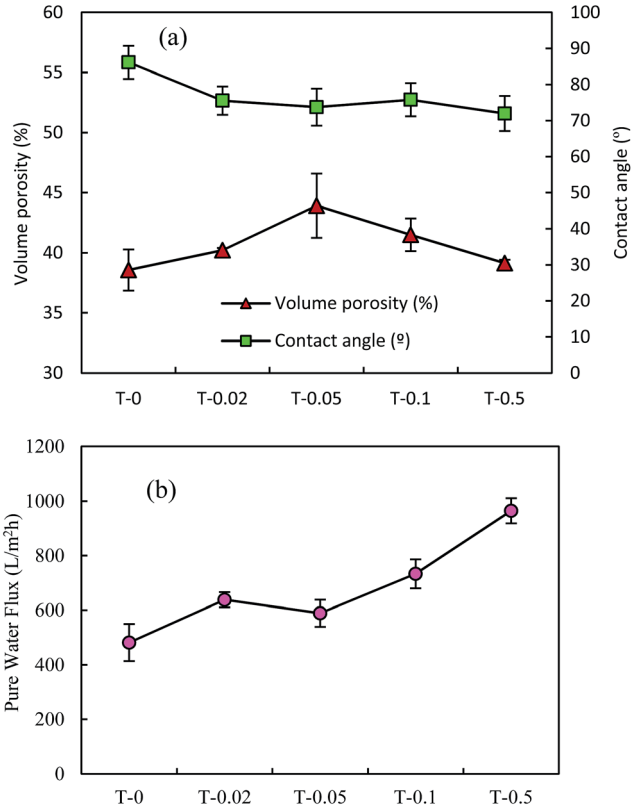

Fig. 5 Comparison of (a) membrane porosity and contact angle, and (b) pure water flux of PVDF/TiO_2 composite membranes and original PVDF membrane.

that the addition of nano-TiO_2 also enhanced the permeability of composite membranes. The increase of the toplayer porosity, hydrophilicity and membrane volume porosity all contributes to the improvement of membrane permeability. Among these, the membrane surface porosity has been well demonstrated to be an important factor impacting the membrane permeability.[24,42] In this study, the membrane surface porosity increased gradually with the addition of nano-TiO_2 according to the membrane formation mechanisms, which can be seen from SEM images (Fig. 1). The increase in porosity directly allowed more water to pass through the membranes and thus presented higher permeability. Therefore, in this study, the enlarged membrane surface porosity was supposed to be a dominant parameter in improving the membrane permeability. Furthermore, the membrane permeability for T-0.1 and T-0.5 was not decreased even though the volume porosity of the membranes declined, which was mainly due to the interconnected macrovoids throughout the cross-sections (see Fig. 1).

3.2. XDLVO analysis

The surface tension parameters and the free energy of cohesion for all the membranes as calculated by eqn (7)–(9) are shown in Table 1. It can be seen that all the membranes have the larger γ^{LW} value compared with the γ^{AB} value, showing that all the membranes feature strong apolar properties. The electron donor component (γ^-) was much higher than the electron acceptor component (γ^+) for all the membranes, suggesting that all the membranes exhibited high electron donor monopolarity, which is in accordance with a previous study.[43] Furthermore, the addition of nano-TiO_2 obviously enhanced the electron donor monopolarity, and γ^- value increased from 5.0 mJ m^{-2} to 12.8 mJ m^{-2} by adding 0.05 wt% nano-TiO_2. It could be also observed from Table 1 that T-0.5 has the highest electron acceptor components (γ^+) and polar components (γ^{AB}) value compared with other membranes, leading to the relatively strong polar properties. In general, surfaces with high electron acceptor capability will interact favorably with surfaces that possess electron-donor functionality, thus causing potentially attractive acid–base interaction.[44]

The LW and AB components of the surface free energy were calculated using eqn (5) and (6), and the sum of LW and AB free energy components for a given material yielded the free energy of cohesion (ΔG_{SWS}). ΔG_{SWS} represents the interaction energy when two surfaces of the same material (for instance, membrane–membrane or foulant–foulant) are immersed in a solvent (*i.e.*, water in this study).[25,42] The negative ΔG_{SWS} value of the membrane surfaces suggests that the membranes are thermodynamically unstable in water, and the more negative the ΔG_{SWS} value is, the stronger the hydrophobicity is. In this study, $\Delta G_{h_0}^{AB}$ was obvious larger than $\Delta G_{h_0}^{LW}$ for all the membranes, implying that the contribution of AB free energy component was more significant compared to LW free energy component. The ΔG_{SWS} value of all the membranes was negative, suggesting that all the membranes were of hydrophobic properties. However, the ΔG_{SWS} value of T-0 was the lowest (−56.1 mJ m^{-2}), and ΔG_{SWS} value of the composite membranes was elevated by adding TiO_2 nanoparticles, which manifests that TiO_2 nanopaticles improved the free energy of cohesion of the membranes, and the improvement was most significant when the concentration of TiO_2 was 0.05 wt% (*i.e.*, T-0.05 membrane). However, with further increase of nano-TiO_2 in the polymer matrix, the aggregation happened, causing the reduction of the free energy of cohesion compared to T-0.05 membrane.

The surface tension parameters of alginate solution with 10 mM NaCl concentration under pH = 6.5 were used to calculate the total interfacial energy *versus* separation distance between alginate and different membranes with eqn (1)–(4). U_{mlc}^{XDLVO} is supposed to determine the alginate-membrane interactions when the alginate is approaching to the membrane surfaces to form fouling. Fig. 6 depicts that the alginate would be subject to the repulsive interaction when getting as close as 30 nm from all the membrane surfaces, and in order to reach the membrane surfaces the foulant must overcome the repulsion interaction energy. The higher the energy barrier is, the harder the initial adsorption is. In this study, the energy barrier between alginate (pH = 6.5, ionic strength = 10 mM NaCl) and T-0–T-0.5 was 0.6, 1.6, 2.4, 1.4 and 1.0 KT, respectively, demonstrating that the addition of TiO_2 nanoparticles improved the interaction energy between foulants and membrane. Therefore, the initial adsorption of the foulants could be mitigated for T-0.02–T-0.5 membranes compared to T-0 membrane.

Table 1 Surface tension parameters and the free energy of cohesion of the membranes (unit: mJ m^{-2})[a]

	γ_s^{LW}	γ_s^+	γ_s^-	γ^{AB}	γ^{TOT}	$\Delta G_{h_0}^{LW}$	$\Delta G_{h_0}^{AB}$	ΔG_{SWS}
T-0	27.8 ± 1.7	0.5 ± 0.4	5.0 ± 2.9	2.6 ± 0.7	30.4 ± 1.7	−0.8 ± 0.4	−55.3 ± 9.1	−56.1 ± 9.1
T-0.02	30.6 ± 0.6	0.4 ± 0.5	11.2 ± 4.8	3.2 ± 1.9	33.8 ± 1.9	−1.5 ± 0.2	−37.3 ± 14.1	−38.8 ± 14.1
T-0.05	34.2 ± 1.5	0.1 ± 0.1	12.8 ± 4.8	1.9 ± 1.1	35.9 ± 2.2	−2.7 ± 0.6	−32.0 ± 8.7	−34.8 ± 8.5
T-0.1	31.0 ± 1.0	0.3 ± 0.2	10.2 ± 2.7	3.5 ± 0.7	34.5 ± 1.5	−1.6 ± 0.3	−40.6 ± 7.5	−42.2 ± 7.8
T-0.5	33.4 ± 1.0	1.2 ± 0.2	9.1 ± 2.2	6.6 ± 0.9	40.0 ± 0.5	−2.5 ± 0.4	−45.5 ± 4.2	−48.0 ± 4.4

[a] Values are given as average ± standard deviation ($n = 4$).

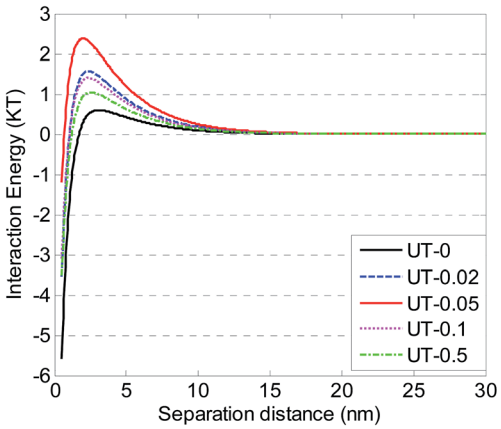

Fig. 6 Variations of interaction energy between membranes and alginate (ionic strength 10 mM NaCl, pH = 6.5).

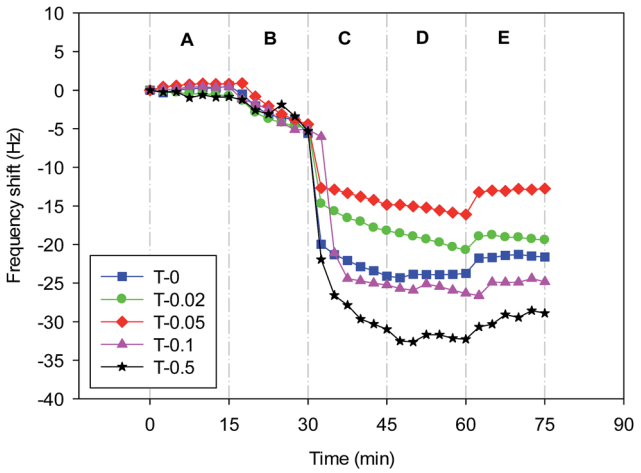

Fig. 7 Representative frequency shifts (7th overtone) by the deposition of alginate sodium onto PVDF and PVDF/TiO_2 coated QCM-D crystals.

3.3. QCM-D analysis

QCM-D provides real-time measurements of molecular adsorption and/or interactions taking place on various surfaces. In this study, QCM-D was used to dynamically verify the deposition of foulants onto different membranes. Fig. 7 displays the real-time frequency shifts of the QCM-D sensor coated with the T-0–T-0.5 recipes as a function of the exposure time. It could be observed that when the foulant solution was injected into the sensor (Phase C), the frequency of all the crystals decreased instantly and the one casted with T-0.5 recipe showed a maximum decline, implying the highest adsorption amount of foulants. The order of frequency decrease during phase C for the five sensors with different membranes coated on is: T-0.5 > T-0.1 > T-0 > T-0.02 > T-0.05, which is unexpectedly inconsistent with that of interaction energy between membranes and alginate solution. The order of repulsive interaction energy barrier between alginate sodium and membranes is: T-0.05 > T-0.02 > T-0.1 > T-0.5 > T-0, which means that even though the interaction energy barrier is higher the membranes are still more favorable of deposition once nano-TiO_2 aggregation happens in the membrane matrix. Washing with background solution and deionized water was performed after the alginate sodium adsorption experiment (Phase D and E) and the frequency of all the sensors increased about 1–5 Hz, indicating that desorption of alginate partly occurred from the membranes. However, the hydrodynamic washing could not remove all the deposited foulants and the initial membrane fouling had formed.

Based on the XDLVO and QCM-D analysis, there is an unexpected result that T-0.1 and T-0.5 has obtained the highest alginate fouling rate rather than T-0, since T-0 had been determined to have the lowest energy barrier with the foulants. Hoek *et al.*[44] has reported that the repulsive interaction energy barrier between foulant and membrane calculated by DLVO theory could be impacted by the membrane roughness, and the repulsive interaction energy barrier between a foulant and a rough membrane is lower than the corresponding barrier for a smooth membrane. Although all the membrane in current study had similar membrane surface roughness, it could be observed from cross-sectional SEM image (Fig. 1) that TiO_2 nanoparticles were aggregated into 0.2–1.0 μm particles and dispersed on the pore wall of T-0.1 and T-0.5, which resulted in increasing the roughness of internal membrane surface. However, the roughness of internal membrane surface could not be detected. Chen *et al.*[45] reconstructed the membrane surface topology based on the statistical parameters obtained from AFM and adopted surface element integration technique to calculate the interaction energy between SMP and the reconstructed rough membrane surfaces in the framework of the XDLVO theory. Their results showed that the great influence of protrusion on the membrane surface could reduce the primary energy barrier height, and an attractive energy region was immediately surrounded by each protrusion as demonstrated in the roughness engendered interaction energy maps.

Therefore, in this study, the aggregated TiO_2 particles dispersed on the pore wall of T-0.1 and T-0.5 are supposed to reduce the interaction energy between foulants and membrane inner surface, inducing more foulants deposition on the membrane pore wall.

4. Conclusions

In this study, physicochemical properties and antifouling behaviours of composite membranes were investigated. The results showed that the addition of TiO_2 could improve the membrane surface porosity, volume porosity, hydrophilicity and permeability. The addition of TiO_2 nanoparticles obviously enhanced the electron donor monopolarity of the composite membranes and increased the repulsive interaction energy barrier between foulants and membrane surfaces, thus improving antifouling ability. The membrane topology obtained from AFM image showed that the incorporation of TiO_2 did not change the average membrane surface roughness. However, the aggregated TiO_2 particles with diameter about 0.2–1.0 μm were dispersed on the pore wall of membrane cross-sections, which was supposed to increase the roughness of membrane inner surface and reduce the repulsive interaction energy barrier between foulants and membrane inner surface. This could result in the deposition of more foulants. In other words, even though the addition of TiO_2 nanoparticles could improve the interaction energy barrier between foulants and membrane surface, the aggregated TiO_2 particles in the membrane matrix could aggravate the membrane pore fouling rate once the concentration of nanoparticles was high enough to form aggregations. Therefore, in this study, the composite membrane with 0.05% TiO_2 nanoparticles had the best performance.

List of symbols

Nomenclature

a	Radius of foulant (nm)
AB	Lewis acid–base interaction energy
e	Electron charge (1.6×10^{-19} C)
EL	Electrostatic interaction energy
$\Delta G_{h_0}^{AB}$	Acid–base interaction free energy components at the separation distance of h_0 (mJ m^{-2})
$\Delta G_{h_0}^{LW}$	Liftshitz–van der Waals interaction free energy components at the separation distance of h_0 (mJ m^{-2})
ΔG_{SWS}	Free energy of cohesion (mJ m^{-2})
h	Separation distance between membrane and foulants (nm)
h_0	Minimum separation distance (0.158 nm)
k	Boltzmann's constant (1.38×10^{-23} J K^{-1})
LW	Lifshitz–van der Waals interaction energy
n_i	Number concentration of ion in the bulk solution
γ^{TOT}	Total surface free energy (mJ m^{-2})
γ^{LW}	LW component of surface free energy (mJ m^{-2})
γ^{AB}	AB component of surface free energy (mJ m^{-2})
γ^+	Electron acceptor component of surface free energy (mJ m^{-2})
γ^-	Electron donor component of surface free energy (mJ m^{-2})
T	Absolute temperature (°C)
z_i	Valence of ion

Greek letters

$\varepsilon_r\varepsilon_0$	Dielectric permittivity of the suspending fluid (F m^{-1})
ξ_m	Surface potentials of the membrane (mV)
ξ_c	Surface potentials of the foulant (mV)
θ	Contact angle (°)
κ	Inverse Debye screening length (m^{-1})
λ	Decay length of AB interactions (0.6 nm)

Subscripts

c	Foulants
l	Bulk liquid
m	Membrane
s	Solid surface

Acknowledgements

This Project is financially supported by China Postdoctoral Science Foundation (2013M540389), National Natural Science Foundation of China (51378371&51308400) and Shanghai Rising-Star Program (14QA1403800).

References

1 M. Elimelech and A. W. Phillip, *Science*, 2011, **333**, 712–717.
2 F. G. Meng, S. R. Chae and H. S. Shin, *Environ. Eng. Sci.*, 2012, **29**, 139–160.
3 P. Le-Clech, V. Chen and T. A. G. Fane, *J. Membr. Sci.*, 2006, **284**, 17–53.
4 G. R. Guillen, Y. J. Pan, M. H. Li and E. M. V. Hoek, *Ind. Eng. Chem. Res.*, 2011, **50**, 3798–3817.
5 M. M. Pendergast and E. M. V. Hoek, *Energy Environ. Sci.*, 2011, **4**, 1946–1971.
6 J. F. Li, Z. L. Xu, H. Yang, L. Y. Yu and M. Liu, *Appl. Surf. Sci.*, 2009, **255**, 4725–4732.
7 W. Y. Li, X. L. Sun, C. Wen, H. Lu and Z. W. Wang, *Front. Environ. Sci. Eng.*, 2013, **7**, 492–502.
8 L. Y. Yu, Z. L. Xu, H. M. Shen and H. Yang, *J. Membr. Sci.*, 2009, **337**, 257–265.
9 P. Aerts, S. Kuypers, I. Genne, R. Leysen, J. Mewis, I. F. J. Vankelecom and P. A. Jacobs, *J. Phys. Chem. B*, 2006, **110**, 7425–7430.
10 L. Yan, S. Hong, M. L. Li and Y. S. Li, *Sep. Purif. Technol.*, 2009, **66**, 347–352.
11 B. Moermans, W. D. Beuckelaer, I. F. J. Vankelecom, R. Ravishankar, J. A. Martens and P. A. Jacobs, *Chem. Commun.*, 2000, 2467–2468.

12 Z. H. Wang, H. R. Yu, J. F. Xia, F. F. Zhang, F. Li, Y. Z. Xia and Y. H. Li, *Desalination*, 2012, **299**, 50–54.
13 L. Brunet, D. Y. Lyon, K. Zodrow, J. C. Rouch, B. Caussat, P. Serp, J. C. Remigy, M. R. Wiesner and P. J. J. Alvarez, *Environ. Eng. Sci.*, 2008, **25**, 565–575.
14 U. Diebold, *Surf. Sci. Rep.*, 2003, **48**, 53–229.
15 S. J. Oh, N. Kim and Y. T. Lee, *J. Membr. Sci.*, 2009, **345**, 13–20.
16 X. C. Cao, J. Ma, H. Shi and Z. F. Ren, *Appl. Surf. Sci.*, 2006, **253**, 2003–2010.
17 Y. N. Yang, H. X. Zhang, P. Wang, Q. Z. Zheng and J. Li, *J. Membr. Sci.*, 2007, **288**, 231–238.
18 Z. W. Wang, X. J. Mei, Z. C. Wu, S. F. Ye and D. H. Yang, *Chem. Eng. J.*, 2002, **193–194**, 77–87.
19 S. Hong and M. Elimelech, *J. Membr. Sci.*, 1999, **132**, 159–181.
20 C. S. Laspidou and B. E. Rittmann, *Water Res.*, 2002, **36**, 2711–2720.
21 B. Q. Liao, D. M. Bagley, H. E. Kraemer, G. G. Leppard and S. N. Liss, *Water Environ. Res.*, 2004, **76**, 425–436.
22 A. Moriya, T. Maruyama, Y. Ohmukai, T. Sotani and H. Matsuyama, *J. Membr. Sci.*, 2009, **342**, 307–312.
23 G. Arthanareeswaran, D. Mohan and M. Raajenthiren, *J. Membr. Sci.*, 2010, **350**, 130–138.
24 Q. Y. Wang, Z. W. Wang and Z. C. Wu, *Desalination*, 2012, **297**, 79–86.
25 C. J. van Oss, *Interfacial Forces in Aqueous Media*, Marcel Dekker, Inc., New York, 1994.
26 C. J. van Oss, *Colloids Surf., A*, 1993, **78**, 1–49.
27 L. Gourley, M. Britten, S. F. Gauthier and Y. Pouliot, *J. Membr. Sci.*, 1994, **97**, 283–289.
28 C. R. Bouchard, J. Jolicoeur, P. Kouadio and M. Britten, *Can. J. Chem. Eng.*, 1997, **75**, 339–345.
29 C. J. van Oss and R. J. Good, *J. Protein Chem.*, 1988, **7**, 179–183.
30 G. Wolanksky and A. Marmur, *Langmuir*, 1998, **14**, 5292–5297.
31 M. Greiveldinger and M. E. R. Shanahan, *J. Colloid Interface Sci.*, 1999, **215**, 170–178.
32 S. Bhattacharjee, A. Sharma and P. K. Bhattacharya, *Langmuir*, 1994, **10**, 4710–4720.
33 V. Vatanpour, S. S. Madaeni, A. R. Khataee, E. Salehi, S. Zinadini and H. A. Monfared, *Desalination*, 2012, **292**, 19–29.
34 T. H. Bae and T. M. Tak, *J. Membr. Sci.*, 2005, **249**, 1–8.
35 F. M. Shi, Y. X. Ma, J. Ma, P. P. Wang and W. X. Sun, *J. Membr. Sci.*, 2012, **389**, 522–531.
36 Y. Wei, H. Q. Chu, B. Z. Dong, X. Li, S. J. Xia and Z. M. Qiang, *Desalination*, 2011, **272**, 90–97.
37 M. Benz, W. B. Euler and O. J. Gregory, *Macromolecules*, 2002, **35**, 2682–2688.
38 A. Salimi and A. A. Yousefi, *Polym. Test.*, 2003, **22**, 699–704.
39 J. S. Andrew and D. R. Clarke, *Langmuir*, 2008, **24**, 670–672.
40 A. Rahimpour, S. S. Madaeni, A. H. Taheri and Y. Mansourpanah, *J. Membr. Sci.*, 2008, **313**, 158–169.
41 Z. X. Ji, X. Jin, S. George, T. Xia, H. Meng, X. Wang, E. Suarez, H. Y. Zhang, E. M. V. Hoek, H. Godwin, A. E. Nel and J. I. Zink, *Environ. Sci. Technol.*, 2010, **44**, 7309–7314.
42 J. A. Brant and A. E. Childress, *J. Membr. Sci.*, 2002, **203**, 257–273.
43 F. Shen, X. F. Lu, X. K. Bian and L. Q. Shi, *J. Membr. Sci.*, 2005, **265**, 74–84.
44 E. M. V. Hoek, S. Bhattacharjee and M. Elimelech, *Langmuir*, 2003, **19**, 4836–4847.
45 L. Chen, Y. Tian, C. Q. Cao, J. Zhang and Z. N. Li, *Water Res.*, 2012, **46**, 2693–2704.